Millimeter-Wave Channel Measurements and Analysis for Statistical Spatial Channel Model in In-Building and Urban Environments at 28 GHz

Junghoon Ko, Yeon-Jea Cho, *Member, IEEE*, Sooyoung Hur, *Member, IEEE*, Taehwan Kim, Jeongho Park, *Member, IEEE*, Andreas F. Molisch, *Fellow, IEEE*, Katsuyuki Haneda, *Member, IEEE*, Michael Peter, Dong-Jo Park, *Member, IEEE*, and Dong-Ho Cho, *Senior Member, IEEE*

***Abstract*—The millimeter-wave (mmWave) band will be a key component of fifth-generation (5G) wireless communication systems. This paper presents radio propagation measurements and analysis investigating the wideband directional channel characteristics of mmWave transmission for in-building and urban cellular communication systems in the 28 GHz band. Based on the measurements, we analyze and model the spatio-temporal channel characteristics such as multipath delay, angular statistics, and path loss. In particular we investigate the clustering of the multipath components, and investigate both the intra-cluster and inter-cluster distributions. Based on these investigations, we present a complete channel model suitable for system simulations in the in-building and urban environments.**

***Index Terms*—Millimeter wave, omni-directional channel measurement, 5G cellular systems, spatial channel model, 28 GHz.**

I. INTRODUCTION

Fifth-generation (5G) cellular systems are expected to use an additional spectrum beyond the traditional wireless bands [2]–[4] that can support more data traffic for various multimedia services. Millimeter-wave (mmWave) bands, between approximately 30 and 300 GHz are candidates to support Gbps-speed wireless connections owing to the availability of large ($\gtrsim$ 1 GHz) bands of contiguous spectra. Consequently, a number of groups have developed mmWave channel models [5]–[7]. In this paper, we focus on characterizing the channel at 28 GHz, which is considered as one of the leading candidates for such 5G systems, since numerous testbeds exist for this band, and the Federal Communications Commission (FCC) in the US in a recent ruling assigned this band for use in 5G [8]. As can be seen from Friis' equation, the free-space path loss (FSPL) increases with the frequency when assuming a constant-gain antenna [9]. For example, systems in the 28 GHz band have 23 dB of additional FSPL when compared to the conventional 2 GHz band. Therefore, the use of a directional high-gain antenna is considered as a solution in mmWave systems.

The propagation characteristics at mmWave frequencies differ from those below 6 GHz, which has a significant impact on system design efforts. For example, in the mmWave bands, reflection is a more dominating propagation mechanism than diffraction compared with those phenomena at lower frequencies [10]. As noted in earlier work [3], mmWave signals do not penetrate most solid materials very well, while signals at lower frequencies can penetrate more easily through buildings. Mmwave transmission can experience significant attenuation in the presence of dense vegetation, and the angular and Doppler spreads are reduced with narrow transmitter and receiver beams. In addition, the number of significant multipath components (MPCs) associated with the mmWave band is much lower than that in the microwave bands, a condition known as channel sparsity [11].

Consequently, wireless systems operating in the mmWave bands will require new air interface designs that are matched to the special propagation characteristics of mmWave channels. While certain models are being developed within 3GPP based on the structures of models below 6 GHz, such as the WINNER II [12] and 3GPP SCM [13], those models were realized under the constraint of a tight deadline, and do not reflect all of the important properties of mmWave channels. A need remains for further investigations and model refinements, e.g., more detailed cluster analyses of multipath channels, as discussed in this paper.

As a first step toward the development of mmWave cellular channel models, it is necessary to analyze the spatio-temporal channel characteristics such as the multipath delay, angular statistics and path loss, and to perform the resulting channel modeling. In this regard, some channel measurement campaigns for outdoor cellular systems at mmWave frequencies have been reported [14]–[17]. In these campaigns, a correlator-based channel sounder with rotating horn antennas was used. These studies, which were based on measurements performed in the USA (Manhattan, New York and Austin, Texas), provided information about important propagation mechanisms and angular spreads (ASs). However, the relative delays of components measured in different directions were not directly measured, but only synthesized with the help of ray-tracing techniques. An omni-directional path loss model based on those measurements was established in [18].

Omni-directional profiles were recreated using ray-tracing techniques to recover the absolute timing [19]. In other work [20], the path loss and delay spread (DS) were compared at different frequencies using omni-directional antennas in urban access scenarios. A model for predicting the path loss from the microwave band to the mmWave band for street microcell environments was also proposed [21]. The channel propaga-

Part of this work was presented at the European Conference on Antennas and Propagation 2015 [1].

tion characteristics were analyzed by using three-dimensional (3D) ray-tracing simulation and compared with measurement campaigns at 28 GHz [22]. In [23], a set of frequency-agile path loss models for urban street canyons was presented and discussed for both line-of-sight (LoS) and non-line-of-sight (NLoS) channels. Several studies investigated the non-stationarity of the path loss from ray-tracing results, presenting a spatially consistent street-by-street path-loss model for use in urban micro-environment (UMi) [24], [25]. For short-range indoor mmWave links, a spatio-temporal statistical channel model was presented in large office rooms, shopping malls, and station scenarios at 60 and 70 GHz [26]. However, as noted in [27], many more measurements are necessary to justify the propagation characteristics in mmWave channels for 5G mobile networks.

Directional channel sounding, which is conducted using a horn antenna, provides impulse responses for a specific combination of transmit and receive directions [14]. In order to obtain (approximate) double-directional characteristics [28], repeated measurements of channel impulse responses (CIRs) are required based on the rotation of such horn antennas to cover all azimuth/elevation directions. The angular resolution is determined by the beam width of the horn antenna; specifically, in our case a 10° beam width. The antenna synthesis allows us to establish the power delay profiles (PDPs) from transmitter (Tx) antenna connectors to receiver (Rx) antenna connectors. Unlike previous measurement campaigns that use ray-tracing to align the delays of directional CIRs, we use our recently-developed delay alignment scheme [29]–[31] with time stamping of each directional CIR. Our constructed channel sounder can thus combine directional CIRs to analyze double-directional power angular-delay profiles and omni-directional path loss and PDPs in the 28 GHz band.

In [31], we used this sounder to measure sevaral sample channels on a university campus and investigated the feasibility of communication systems in the 28 GHz band based on these measurements. The paper presents various features including foliage effects, signal outages, path loss and outdoor-to-indoor (O2I) conditions on the campus of the Korea Advanced Institute of Science and Technology (KAIST) for outdoor scenarios. In the current paper, we present the results of two much more extensive measurement campaigns in different environments, i.e., an urban environment in downtown Daejeon, Korea, and an indoor lounge-type environment on the KAIST campus. The emphasis of the current paper is on the channel parameters, which - due to the larger number of measurement points - are also more statistically significant.

To summarize the main contributions, this paper presents a wideband double-directional channel sounding campaign at 28 GHz along with channel parameters based on clustered channel models for two important cellular scenarios, i.e., an urban microcell and an open indoor hall mainly for NLoS scenarios. The remainder of the paper is organized as follows: Sections II and III describe the sounder setup and the channel sounding settings, respectively. Section IV details the channel parameter extraction procedure, and conclusions are presented in Section V.

TABLE I
28 GHz Channel Sounder Specifications

Parameters	Values
Carrier Frequency	27.925 GHz
PN Sequence Type	11th order m-sequence
PN Sequence Rate	250 Mcps
DAQ Sampling Rate	1 Gsps
Horn Antenna Gain	24.5 dBi
Horn Antenna HPBW	10 degrees
Antenna Polarization	Linear polarization
Transmit Power	29 dBm max

II. Synthesized Omni-directional Channel Sounding

A. Directional Millimeter-wave Channel Sounder

The radio channel measurement at 28 GHz was conducted using a wideband channel sounder capable of estimating the PDP over a long Tx-Rx distance. The core of the sounder is digital correlation performed as a post-processing step, which provides multipaths with a 4 ns delay resolution by exploiting 250 Mega chip-per-second (Mcps) pseudo-random (PN) sounding sequences. The PN sequence consists of an m-sequence produced by an 11th-order shift register with an 8.188 μs sequence duration. The m-sequences are modulated to produce a rectangular-shaped binary-phase-shift-keying (BPSK) signal. Horn antennas with a 10° half-power beam width (HPBW) in both the azimuth and elevation planes and a gain of 24.5 dBi are installed on the Tx and Rx sides. On the Rx side, the sampling rate of an analog-to-digital converter (ADC) is one giga-samples per second (Gsps), performing four times oversampling at the baseband sequence rate. The Tx and Rx sides have their own external reference clocks which are synchronized by a common trigger signal generated by a function generator fed to the two sides through a cable connection. Table I shows the measurement system specifications; see also the literature [31] for more details.

Given that the sounder is equipped with directional horn antennas, the maximum measurable path loss value is approximately 160 dB, typically corresponding to Tx-Rx distances of a few hundred meters. However, it requires antenna scanning over all possible beam pointing directions due to the narrow beam width of the antennas - unlike a sounder using an omni-directional antenna. Both the Tx and Rx sides are equipped with antenna steering modules based on stepper motors that automatically control the beam pointing direction over the azimuth and elevation angles. Directional measurements are performed at every 10° over the azimuth and elevation angles, leading to a maximum of 36 and 13 angular bins, respectively. Note that angular bins near both ends, $60^{\circ} \sim 90^{\circ}$ and $-90^{\circ} \sim -60^{\circ}$, in the elevation plane receive such a low level of power that they can be neglected during the measurement process.

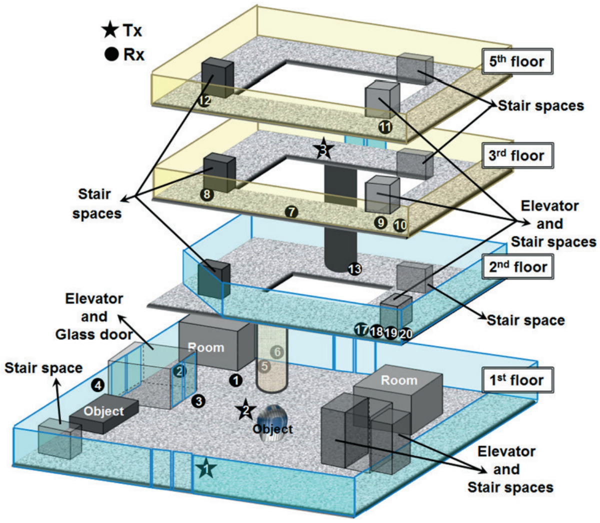

Fig. 1. Floor plan of the five-story building showing the Tx and Rx antenna locations. Only a part of the total 35 Rx antenna locations are marked.

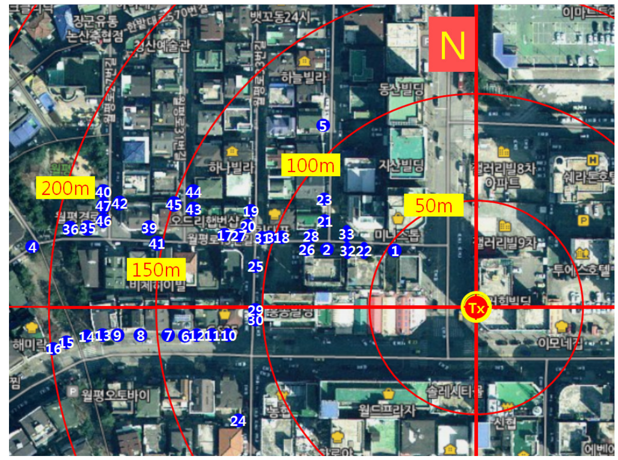

Fig. 2. Map of the Tx and Rx locations in the urban measurement site.

B. Synthesized Omni-directional Power Delay Profile

We use a delay synchronization technique when undertaking the directional channel measurements by determining the time stamps of the Tx time for each directional measurement. Details of this technique are described in [31]; we repeat here the essentials for the convenience of the reader. First, the directional PDPs with noise reduction are obtained from measurements of each beam channel. In the channel sounding for each Tx and Rx steering angle, fifty consecutive directional impulse responses are measured and recorded. Then, the synchronization technique allows each directional PDP to be aligned with the same relative propagation delay of the channel, making it possible to derive double-directional PDPs covering all solid angles of the antenna pointing directions. Note that the Tx and Rx are not phase-synchronized, and time synchronization is done only within less than a chip period, i.e., approximately the inverse of the bandwidth. Thus, synchronization is realized by time-aligning the impulse responses in different directions, which does not imply coherent processing. Finally, omni-synthesized PDPs are obtained by choosing the paths having the maximum level of power at each resolvable delay to avoid overestimating the path power. The synthesis algorithm is experimentally verified by comparing the omni-synthesized PDP with a measured PDP using an omni-directional antenna in [29].

III. Channel Sounding Campaigns

Channel sounding was conducted in two sites, one representing an indoor scenario similar to a small shopping mall and another being an outdoor urban environment in Daejeon, South Korea.

A. In-building Environment

The first channel sounding was carried out inside a five-story building on the KAIST campus. Figure 1 shows the measurement site for the in-building scenario. We performed the channel sounding in the space around the atrium. The Tx antenna was positioned either on the first floor, termed Tx positions 1 and 2, or on the third floor, referred to as Tx position 3. Measurement campaigns were carried out for various Rx positions on the same and different floors, with 35 Tx-Rx links in total. The measurement scenario is defined via the indices of the Rx antenna locations, including both LoS and NLoS channels. For example, the LoS Rx positions are in front of Tx position 3, while the NLoS Rx positions are behind the stairs or in the corridors. The Tx-Rx distance ranged from 10 m up to 40 m. The range of the antenna steering angles was from 0° to 360° in the azimuth on both the Tx and Rx sides. The elevation angle of the Tx antenna was set to the strongest signal direction during the first antenna scanning process. On the Rx side, the elevation angle was scanned within the range of $\pm 60^\circ$ according to the measurement environment.

B. Urban Environment

The second channel measurement was performed in a densely built-up urban environment in downtown Daejeon, South Korea and was focused on a sector for one main direction of the Tx. The Tx antenna was placed on the fifth floor of a building at a height 15 m above the ground. Figure 2 depicts a satellite map of the Tx and Rx antenna locations of the channel sounding. The sounding was carried out for 47-NLoS Rx antenna locations in total, among which 38 locations provided meaningful channel data sets with signals observed; the channels at Rx positions 4, 5, 16, 17, 25, 26, 27, 31 and 46 shown in Fig. 2 experienced outages and thus were not used for further analysis. The criterion for a signal outage is whether the received signal power is weaker than the minimum detectable signal level. Strictly speaking, this refers to "channel sounding outage" rather than "communication outage:" the communication outage is related to the bandwidth, transmit power, and beamwidth of the communication system relative to that of the sounding system. More precisely, what we call a signal outage here is a path loss of more than 160 dB, a value that might or might not coincide with the communication outage. However, for the sake of simplicity, "signal outage" is henceforth used in lieu of "channel sounding outage" in this paper.

The receivers at Rx positions 4, 16, and 46 experienced a signal outage due to their long distances from the Tx position. For the other Rx locations (5, 17, 25, 26, 27, 31), however, a signal outage occurred despite the fact that the distances between the Tx and Rx locations were not great. This occurred because there are no effective reflectors on the propagation path; the signal level of the reflected path is dependent on the reflection conditions, such as the material, thickness, and the surface roughness of the reflector, the incident (reflection) angle, and the number of reflections. In mmWave systems, due to the absence of diffraction as an efficient propagation mechanism and thus stronger shadowing variations compared with centimeter-wave (cm-wave) systems, the probability that locations even close to the base station (BS) can undergo an outage is increased. Other locations at the same Euclidean distance from the BS might receive strong signals due to the presence of strong reflectors. Some measurements regarding such cases were conducted and discussed in earlier work [31].

In particular, near a street crossing (Rx positions 17, 25, 27, and 31), because the signals experienced multiple reflections on the propagation path, the received power level was not large enough to detect. Therefore, the increased margin might be required against the higher shadowing outage in this case. In addition, it can be seen that if the receiver moves along a straight line of street canyons (Rx positions 10 - 6 - 8 - 14), the signal was still received without a signal outage even though the distance increased from 100 m to 200 m. This indicates that it is possible to receive a signal at a considerable distance when the presence of a definite reflector is maintained. This phenomenon known as the wave guiding effect was also presented in [24].

The measured channels include various scattering environments in an NLoS setting with the Tx-Rx distance ranging from 43 m to 209 m. The $0°$ azimuth was set to the west at all Tx and Rx antenna locations. The ranges of the antenna scanning angles were from $-60°$ to $60°$ and $-40°$ to $10°$ in the azimuth and elevation domains, respectively, on the Tx side. For all Rx positions, all meaningful signals were observed within only these angle ranges. Therefore, to reduce the required measurement time, the channel measurements for other ranges in the azimuth and elevation angle axes were not considered. The scanning ranges in the azimuth and elevation domains on the Rx side were from $0°$ to $360°$ and $-60°$ to $60°$, respectively.

IV. Characterization of 28 GHz channels

In this section, the spatio-temporal characteristics and path loss of the 28 GHz channel are presented in the two measurement sites. They are analyzed based on the discrete form of the synthesized omni-directional PDPs. The spatio-temporal analysis includes the statistics of cluster and multipath component (MPC) delays, power distribution, delay spread (DS) and angular spread (AS) as well as the number of clusters. An automatic clustering algorithms is introduced to derive cluster parameters. For the convenience of the readers, a list

TABLE II
List of Symbols

i	i-th pointing angle at Tx.
j	j-th pointing angle at Rx.
l	l-th channel tap with respect to an omni-directional PDP.
τ_l	Excess delay of the l^{th} channel tap.
ϕ^l_{AoD}	Azimuth AoD associated with the l-th channel tap.
θ^l_{AoD}	Elevation AoD associated with the l-th channel tap.
ϕ^l_{AoA}	Azimuth AoA associated with the l-th channel tap.
θ^l_{AoA}	Elevation AoA associated with the l-th channel tap.
$L_{i,j}$	Number of channel taps at the $\{i,j\}$-th angle bin.
L	Number of channel taps with respect to an omni-PDP.
$\mathcal{C}_L$	Set of channel taps.
$P_{i,j}(\cdot)$	Power delay profile for the $\{i,j\}$-th pointing angle.
N_{Tx}	Number of angle bins at the Tx.
N_{Rx}	Number of angle bins at the Rx.
k	k-th cluster.
K	Number of clusters.
L_k	Number of channel taps associated with the k-th cluster.
$\mathcal{C}_k$	Set of channel taps associated with the k-th cluster.

of symbols used in this paper is shown in Table II. In the characterization, we consider taps or bins in the angular and delay domains; the delays τ_l of MPCs fall into one of the delay bins spaced in 4 ns step, while the azimuth and elevation angle of departure (AoD), ϕ^l_{AoD} and θ^l_{AoD}, and those of angle of arrival (AoA), ϕ^l_{AoA} and θ^l_{AoA}, are described as being in one of the angular bins with $10°$ step size.

A. Path Loss Analysis

Path loss is a fundamental component of radio channel models for estimating the link budget and coverage in a cellular network. From measured data, the path loss for each location was estimated as

$$PL = P_{Tx} - P_{Rx} + G_{Tx} + G_{Rx}, \tag{1}$$

where P_{Tx} is the transmit power, and P_{Rx} is the received power derived by integrating the energy of the paths in the synthesized omni-PDP. In addition, G_{Tx} and G_{Rx} are the gains of the horn antennas used during the transmission and reception processes, respectively. For our measurement system, P_{Tx} = 29 dBm and G_{Tx} = G_{Rx} = 24.5 dBi. The omni-directional path loss can be successfully determined by integrating all of the powers of the synthesized paths; see earlier work in the literature [32].

Two popular modeling approaches to fit measured PLs have been suggested. One approach is based on a close-in free-

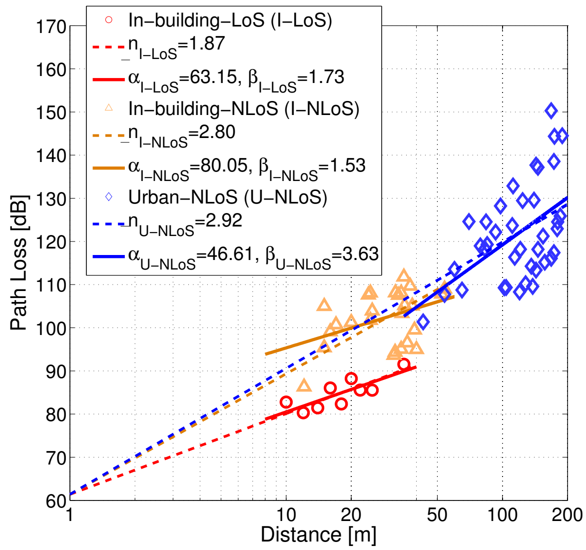

Fig. 3. Alpha-beta (floating-intercept) and close-in free-space reference-distance path loss models, and scatter plots for in-building and urban environments.

space-reference-distance (CI) path loss model, and the model can be combined with log-normal shadowing, as follows:

$$\overline{PL}\,(d)\,[dB] = PL_F\,(d_0) + 10 \cdot \overline{n}\,\log\left(\frac{d}{d_0}\right) + X_\varsigma, \qquad (2)$$

where d is the two-dimensional (2D) Euclidean distance in meters, d_0 is the reference distance in meters, and PL_F represents the FSPL. The linear slope $\overline{n}$ is well known as the path loss exponent (PLE), and the shadowing effect is described by a Gaussian random variable (in dB) X_ς with a zero mean and standard deviation of ς. The reference path loss can be obtained from the Friis formula at $d_0 = 1$. In our case, $PL_F\,(1m) = 61.4$ dB.

An alternative modeling approach which has been used in the well-known Okumura-Hata model [33], the WINNER II model [12] and the 3GPP SCM [13] as well as the COST 2100 model [34] is to estimate the two parameters: the slope and the intercept directly from the data. This model, known as the alpha-beta (AB) or floating-intercept (FI) path loss model, can be combined with log-normal shadowing as follows:

$$\overline{PL}\,(d)\,[dB] = \alpha + 10 \cdot\; \beta\log\left(d\right) + X_\sigma, \qquad (3)$$

where α and β are the least-square fits of the floating intercept and the slope. In addition, the shadowing effect X_σ (in dB) is considered as a Gaussian random variable with zero mean and standard deviation σ. The accuracy of the path loss model can be improved, in principle, by including the fact that some measurement points are "censored," i.e., have receive power below the sounder sensitivity level [35]. However, because determination of the sensitivity level was difficult in the rotating-antenna setup, this is not exploited in our evaluations.

Figure 3 shows a scatter plot of the path loss of the in-building LoS and NLoS channels. With a reference distance of 1 m, the minimum root-mean-square (RMS) error fit of

TABLE III

THE PATH LOSS PARAMETERS

	In-building LoS	In-building NLoS	Urban NLoS
d [m]	$10 < d < 40$	$10 < d < 60$	$40 < d < 200$
d_0 [m]	1	1	1
$\overline{n}$	1.87	2.80	2.92
ς [dB]	2.07	6.18	9.89
α [dB]	63.15	80.05	46.61
β	1.73	1.53	3.63
σ [dB]	2.06	5.79	9.83

(2) with the measurements gives PLEs of 1.87 and 2.80 in the LoS and NLoS conditions, respectively. Figure 3 also shows a path loss plot of the urban NLoS channels, showing that their PLE is 2.92. When undertaking the fitting of (3) in our measurements, we obtain $\{\alpha = 63.15, \beta = 1.73\}$ and $\{\alpha = 80.05, \beta = 1.53\}$ in the in-building LoS and in-building NLoS cases, respectively, and $\{\alpha = 46.61, \beta = 3.63\}$ in the urban NLoS case. The parameter β $(= 1.53)$ is low for the NLOS case, though it is physically possible (together with a higher offset α) given the propagation mechanism of waveguiding. The model parameters for (2) and (3) are listed in Table III for the two measurement sites with the distance range of validity.

We compared the path loss results of this work with those of other measurements at 28 GHz. In one earlier case [16], the path loss parameters $\{\overline{n} = 3.4, \alpha = 79.2, \beta = 2.6\}$ were obtained for outdoor NLoS measurements. For the indoor NLoS case in another study [36], the parameter values of $\{\overline{n}, \alpha, \beta\}$ were 2.7, 51.3 and 3.5, respectively. Note that in those papers, the omni-directional path loss was synthesized by superimposing all of the directional PDPs obtained from beam-pair measurements. Although the measurement environment and the method used for the path loss analysis are different, the parameter values of the CI model are similar to each other in both indoor and outdoor scenarios. On the other hand, the parameter values for the AB path loss model are quite different in the two scenarios; the existence of two parameters means that the two parameters can appear quite differently even though the curves they describe are quite similar within the distance range of validity. Note that with any measurement-based model, it is important for the distance range in which the AB model is applied be limited to the range in which the measurement campaigns are conducted. The single parameter n describing the CI model can be more easily compared between different measurement campaigns.

There are also many more path loss measurement results for indoor environment at mmWave frequency bands. For 73 GHz indoor measurements, PLEs were 1.3 and 3.2 for LoS and NLoS scenarios, respectively, when applying the CI path loss model [36]. For the NLoS case when using the AB path

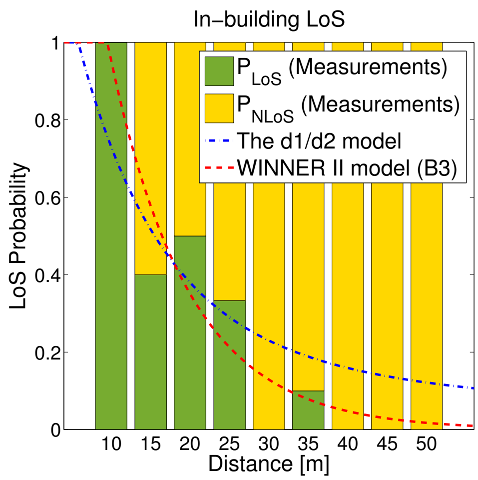

Fig. 4. LoS probability models of in-building LoS measurements.

loss model, the parameter values of $\{\alpha, \beta\}$ were 76.3 and 2.7, respectively. In [37], PLEs were observed under various propagation conditions at 58 GHz, which were in the range 0.18 - 1.17 for LoS environments, and were in the range 2.67 - 5.45 for NLoS environments. Note that the AB path loss model was used in that paper. [38] and [27] provide a summary of PLEs presented in the previous literatures for indoor environments at 60 GHz. In that paper in which the CI model was adopted, the average PLEs were 1.6 and 1.7 for office LoS and generic LoS environments, respectively. On the other hand, in the case of NLoS measurements, the values were 3.4 and 3.3 for office and generic environments, respectively. In addition, it was noted that there is no significant difference of the PLE between the use of directional or omni-directional antennas [27].

In addition, the LoS probability is analyzed to complete the path loss model from the measurement data for an in-building LoS environment. The LoS probability represents how often there is a direct path between the Tx and Rx, which has a frequency-dependent feature [39]. For the LoS probability characteristic, two distance-dependent models are considered in this work. The first model is the d1/d2 model which is a distance-dependent exponential function with two parameters d_1 and d_2 [40],

$$P_{LoS}\left(d\right) = \min\left(d_1/d, 1\right)\left[1 - \exp\left(d/d_2\right)\right] + \exp\left(d/d_2\right), \quad (4)$$

where d is the 2D distance in meters between Tx and Rx. The second model is the LoS probability model used in WINNER II in scenario B3 (indoor hotspot), as follows [12]:

$$P_{LoS}\left(d\right) = \begin{cases} 1, & d \leq d_3 \\ \exp[-\left(d - d_3\right)/d_4], & d > d_3 \end{cases}. \quad (5)$$

For both models, the parameters can be optimized to fit a given set of data according to a minimum RMS criterion. From our data, we obtain $\{d_1 = 5.83, d_2 = 9.61, d_3 = 9.52, d_4 = 10.0\}$ in the shopping mall-like indoor environment: the measurement samples were divided into bins of 5 m size, and the LoS probability was calculated as the ratio of the number of LoS points to that of LoS plus NLoS points for each bin from the measurement results. In Fig. 4, the two models are compared with the measurement data. Although the WINNER model (RMSE = 0.1137) in (5) provides better performance than the d1/d2 model (RMSE = 0.1754) in (4), there is a need for additional and complementary measurement campaigns for an accurate comparison. Moreover, the parameters for each model can be updated from additional measurements. Based on the parameters, such as path loss, shadow fading (signal outage) and LoS probability, the deployment density of the BSs can be planned.

B. Clustering the MPCs

It is well established that MPCs have a tendency to occur in *clusters*, i.e., groups of MPCs that have similar angular and delay characteristics. Such clusters can often be attributed to physical (geometrical) groups of objects that are in close proximity to each other, and are surrounded by empty space. Clusters can be identified either visually in the multi-dimensional power spectrum [41] or automatically using clustering algorithms. In this paper, we use the KPowerMeans algorithm [42] for the iterative automatic clustering of the measured MPCs at a given location, which has been used in a large number of papers investigating cluster-based channel models. This algorithm uses the multipath component distance (MCD) as a metric for clustering by minimizing the sum of the MCDs between MPCs and their cluster centroids. To determine the optimum number of clusters, the Kim-Park (KP) method [43] is used. Figure 5(a) shows the exemplary clustering of MPCs using the KPowerMeans algorithm, in which three clusters can be observed.

In the COST 259 models, e.g., [44], [45], the number of clusters is a random variable whose distribution parameters depend on the environment and propagation scenario. Our measurements support this model given that the average numbers of clusters were 3.52 and 4.58 for the in-building and urban scenarios, respectively. The corresponding cumulative distribution functions (CDFs) of the number of clusters are shown in Figs. 5(b) and 5(c), where the positive Poisson distributions are also illustrated as the best fit for both the in-building and urban measurement data. Note that the average numbers of clusters for our in-building and urban scenarios are significantly smaller than those from the results below 6 GHz, such as 3GPP [13], WINNER II [12] and ITU-R [40], with channel sparsity (also called multipath sparsity) at the mmWave bands. The channel sparsity conditions have noticeable effects on spatial multi-user (MU) multiplexing in (massive) MIMO communication systems. In [46], it was shown that the number of independent MPCs at mmWave frequencies is typically limited and that the channel vectors are not independent and identically distributed (i.i.d) Rayleigh but rather correlated fading channels. In another study [47], it was found that when users are close to each other, they share the same cluster. This results in a spatial correlation between user channel vectors, with subsequent deterioration of the optimal system performance in realistic designs of the MU-

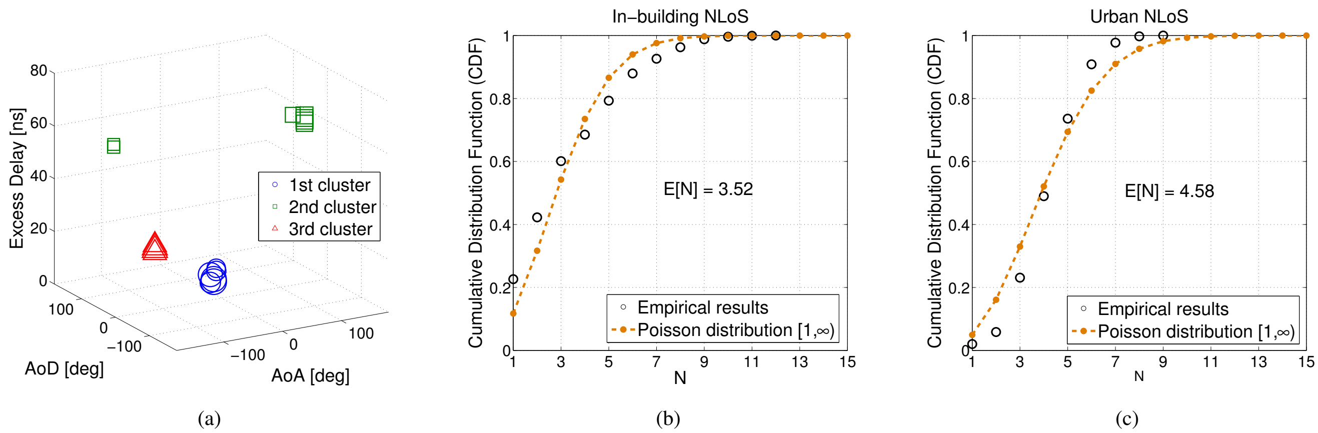

Fig. 5. (a) An example of clustering algorithm: three clusters of MPCs from the synthesized omni measurements at the position of RX 13. Cumulative distribution functions of the number N of clusters for (b) the in-building NLoS environment and (c) urban NLoS environment.

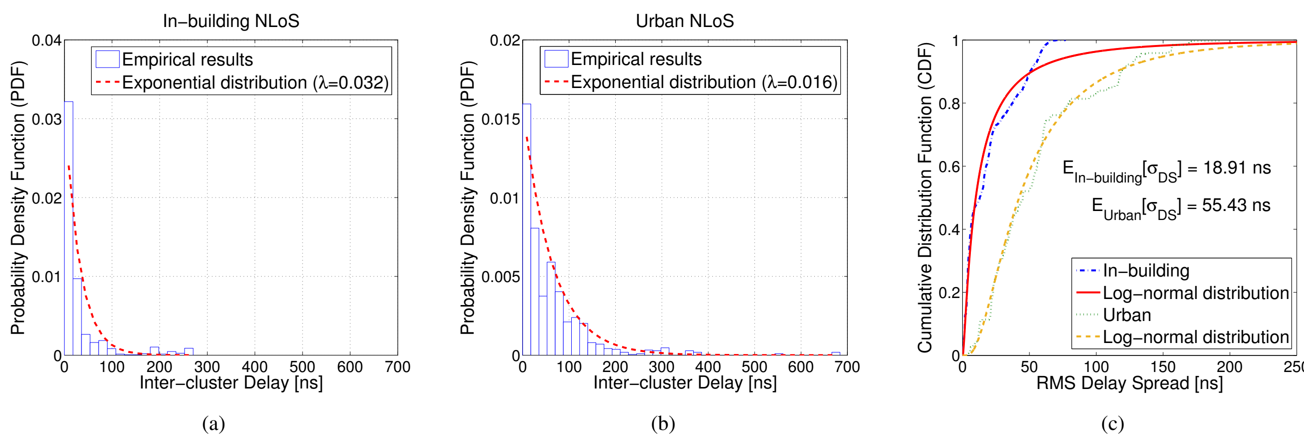

Fig. 6. Probability density functions of inter-cluster delays for (a) the in-building NLoS environment and (b) urban NLoS environment. (c) Cumulative distribution functions of RMS delay spreads for the in-building and urban NLoS environments.

MIMO systems, especially in mmWave outdoor propagation channels.

C. Cluster Characteristics in the Delay and Power Domains

1) Cluster delays: The delay-domain characteristics of clusters are analyzed based on inter-cluster delays, root-mean-square delay spread (RMS DS), and PDPs. Following the well-known Saleh-Valenzuela model [48], we model the inter-cluster delays as random variables. Figures 6(a) and 6(b) show histograms of the inter-cluster arrival times for all clusters in the in-building and urban scenarios. It was found that the exponential distributions are well matched with the histograms and that the decay rate parameter values are 0.032 ns^{-1} and 0.016 ns^{-1} for the in-building and urban environments, respectively.

The cumulative distribution functions (CDFs) of the DSs in the in-building and urban scenarios are illustrated in Fig. 6(c), where the log-normal distributions have been overlaid as the best fit when considering the in-building and urban measurement data together, revealing that most channels have DSs lower than 100 ns and 200 ns for the in-building and urban environments, respectively. The average corresponding DSs are 18.91 ns and 55.43 ns for the in-building and urban scenarios, respectively. The present DSs of omni-PDPs are not longer than those of currently used cellular frequencies [12], [13]. This is in good agreement with the fact that the distances between Tx and Rx at mmWave frequencies are shorter than at cmWave or current cellular frequencies. Because the DS increases approximately with the square root of the distance (compare [45] and [49]), a reduced DS is in line with expectations.

Note that the average DS value (55.43 ns) for the outdoor scenario from our omni-directional measurements is significantly greater than the DS value (17.4 ns) in an earlier study [16], where the directional DS was computed. This stems from the fact that as more signals are transmitted in multiple directions, more signals are received within a wide range in time. This was also noted in [31], where a comparison between omni-directional and directional DSs was conducted. In another study [50] as well, both directional and omni-directional RMS DS values were introduced, showing that in such an environment that the mean DS values are 17.4 ns and 40.9 ns, respectively at 28 GHz. The difference in the mean DS values between our work and the aforementioned study [50] is due to the difference in the geometry of environment and possibly the means used to obtain the values. Note that

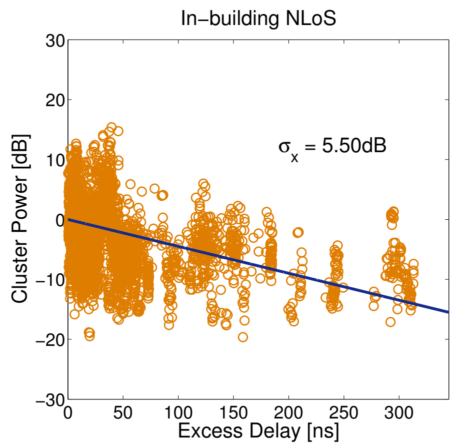

(a)

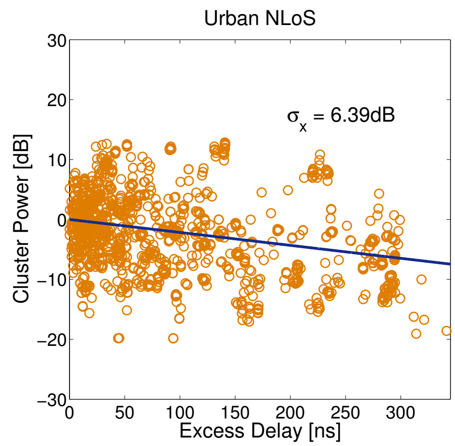

(b)

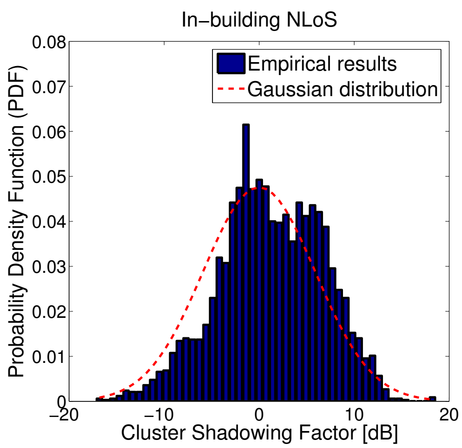

(c)

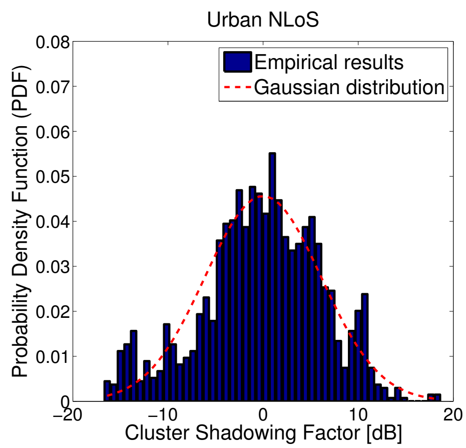

(d)

Fig. 7. Excess delay vs. normalized cluster power: (a) the in-building NLoS and (b) urban NLoS environments. PDF of cluster shadowing factors for (c) the in-building NLoS and (d) urban NLoS environments.

the DS values in [50] use ray tracing to synthesize their omni-directional profiles, as mentioned in that paper.

However, in the indoor measurements, the average DS value in this work is similar to those from the directional measurements in [36], which were 18.91 ns and 17.7 ns, respectively. This may be due to the fact that the propagation space is relatively small such that the signals are received within a limited time range, even in the case of omni-directional transmission. Further, note that the measurement environment in that study [36] (a common office) is somewhat different from those in this work (in-building locations similar to a small shopping mall). In short, the average DS value on the Rx side becomes significantly larger when transmitting multiple beams as compared with the case of single beam transmission, especially in an outdoor environment.

2) Cluster power: In general, the power of clusters depends on their excess delays, and this relationship should be determined by the measurements. In many cases [45], [48], [51], an exponentially decaying PDP is considered as a good model, and this is also shown in our measurements. Figures 7(a) and 7(b) illustrate the PDPs of our in-building and urban channels from which the single-slope-exponential power decay of the cluster powers was observed. Here, the cluster powers were normalized with respect to the power of the first cluster at each measurement position. The decay constants of the cluster power in dB per nanosecond for the in-building and urban environments are -0.045 dB/ns and -0.022 dB/ns, respectively. Additionally, the probability density functions (PDFs) of the cluster shadowing factor for each case are presented in Figs. 7(c) and 7(d), respectively, with the Gaussian distribution as their best fit.

3) Intra-cluster delays: The large bandwidth of mmWave systems to achieve the extremely high delay resolution calls for an accurate model of intra-cluster MPC delays (called sub-path delays in the 3GPP SCM). Histograms of the inter-path delays within each cluster from measurements in both the in-building and urban environments are shown in Figs. 8(a) and 8(b), respectively. They follow an exponential distribution in both cases and are thus well-aligned with the Saleh-Valenzuela model. The intra-cluster DS $\sigma_{DS,k}$ due to subpaths for the k-th cluster is computed using the paths in the cluster. The mean (i.e., averaged over different clusters) values of the intra-cluster DS, denoted by $\sigma_{DS,c} = E\left[\sigma_{DS,k}\right]$ are 3.90 ns and 12.86 ns, in the in-building and urban scenarios, respectively. The corresponding CDFs are also plotted in Fig. 8(c).

In the statistical SCM, we can consider the delay, AoD and

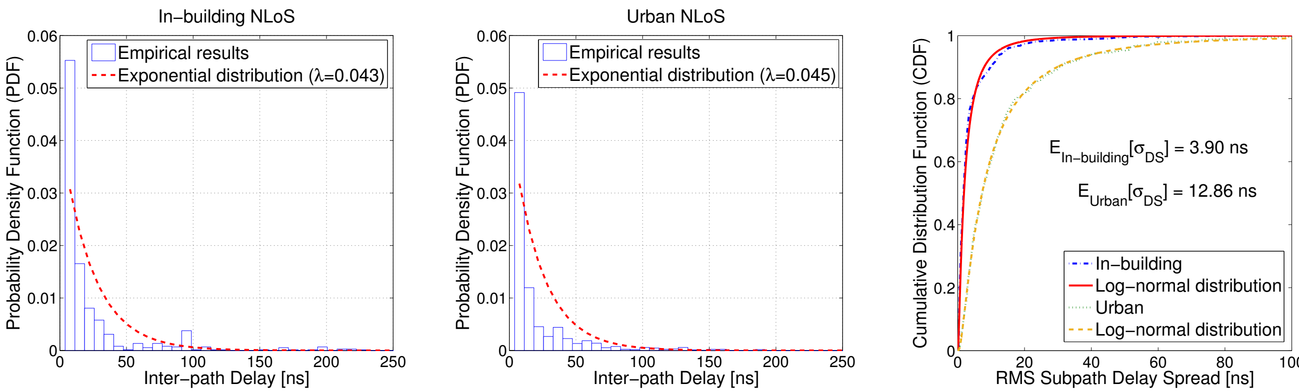

(a) (b) (c)

Fig. 8. Probability density functions of inter-path delays within each cluster for (a) the in-building NLoS and (b) urban NLoS environments. (c) CDFs of the intra-cluster DS for the in-building and urban NLoS environments.

AoA of the subpaths as random variables or fixed values. If we model the intra-cluster delay v as a random variable, its probability density function (PDF) is an exponential function:

$$f_v\left(v\right) \triangleq \frac{1}{\sigma_{DS,c}} \exp\left(-\frac{v}{\sigma_{DS,c}}\right), \tag{6}$$

where $v > 0$. We also denote the CDF of $f_v\left(v\right)$ as $F_v\left(v\right)$. Because the cluster size is finite in actual environments, it makes sense to define an effective interval for the intra-cluster delays. In this regard, we use a constrained version of $f_v\left(v\right)$ to generate clear clusters and to limit the cluster size in the delay domain, as follows:

$$f_{v'}\left(v'\right) \triangleq \begin{cases} \frac{f_v\left(v'\right)}{F_v\left(v^{\text{upper}}\right)}, & 0 \leq v' \leq v^{\text{upper}} \\ 0, & v' > v^{\text{upper}}, v' < 0 \end{cases}. \tag{7}$$

In this equation, v^{upper} is determined to satisfy the following condition:

$$\sqrt{E\left[v'^2\right] - \left(E\left[v'\right]\right)^2} = c_1\sigma_{DS,c}.$$

We set the above parameter c_1 to 0.95 and assume that the power of a cluster is equally divided between their subpaths.

D. Cluster Characteristics in the Spatial Domain

In double-directional channel models, angle models are based on circular AS statistics obtained from real-world measurements. Accordingly, 0° is newly defined as the mean direction used for the computation of the circular AS in contrast to the angle defined during the channel sounding process.

1) Cluster AoDs/AoAs: Figure 9 shows the distributions of the measured cluster AoA and AoD in the in-building and urban environments. As the best model with the corresponding mean square error (MSE) criterion, a Laplacian distribution is overlaid. It should be noted that the best-fit model at 28 GHz differs from that in the conventional cellular bands under 6 GHz, where wrapped Gaussian distributions are used [12].

Additionally, the statistics pertaining to both the inter-cluster AoD and AoA spreads (ASD and ASA) were analyzed in the in-building and urban environments. With an arbitrary angle shift denoted by Δ, the inter-cluster ASA and ASD, σ_{ASA} and σ_{ASD}, are calculated by taking into account the circularly symmetric properties of azimuth angles. The measured inter-cluster ASA and ASD are plotted in Fig. 10(a) in the form of CDFs. The average inter-cluster ASDs in the in-building and urban measurements are 15.02° and 7.68°, respectively, while the average corresponding ASAs are 32.16° and 31.39°, showing greater values than the ASDs. It was found that these spread values are slightly lower than those of the current cellular frequencies [12], [13]. It was also found from the measurements that the standard deviation of the cluster AoA from the reference direction, i.e, 0°, depends on the cluster power relative to the total power. Note that this relationship was introduced in [52]. Figures 10(b) and 10(c) illustrate the curve fits for the distributions of cluster AoAs obtained using uniformly spaced bins of the received power in the in-building and urban environments, respectively. The corresponding standard deviation, $\sigma_{n,AoA}$, can be expressed as follows:

$$\sigma_{n,AoA} = A \cdot \left[1 - \exp\left(B \cdot \left|P_{n,dBr}\right|\right)\right], \tag{8}$$

where $P_{n,dBr}$ (< 0) is the relative power of the n-th cluster in dBr with respect to the total received power and the parameters A and B are specific to each environment [53].

2) Intra-cluster AoDs/AoAs and subpath power: The intra-cluster ASD and ASA are used to determine the intra-cluster AoD/AoA offsets, $\delta_{n,m,AoD}$ and $\delta_{n,m,AoA}$ for the n-th cluster and $m = 1, 2, \ldots, M$, with M being the number of subpaths, considered as a fixed parameter for a specific environment or random variables. The power of a cluster could be equally divided among M subpaths, or more precisely, the power of each MPC within a cluster can be modeled as random variables. In Fig. 11, the PDFs of normalized power levels belonging to each MPC are presented from our measurements in the two environments. The normalized power refers to the ratio of the power of each MPC to the power of the corresponding cluster. As shown in Fig. 11, when sorting the normalized power levels in descending order, the power of the each MPC in dB scale within a cluster follows the truncated log-normal distribution in both cases.

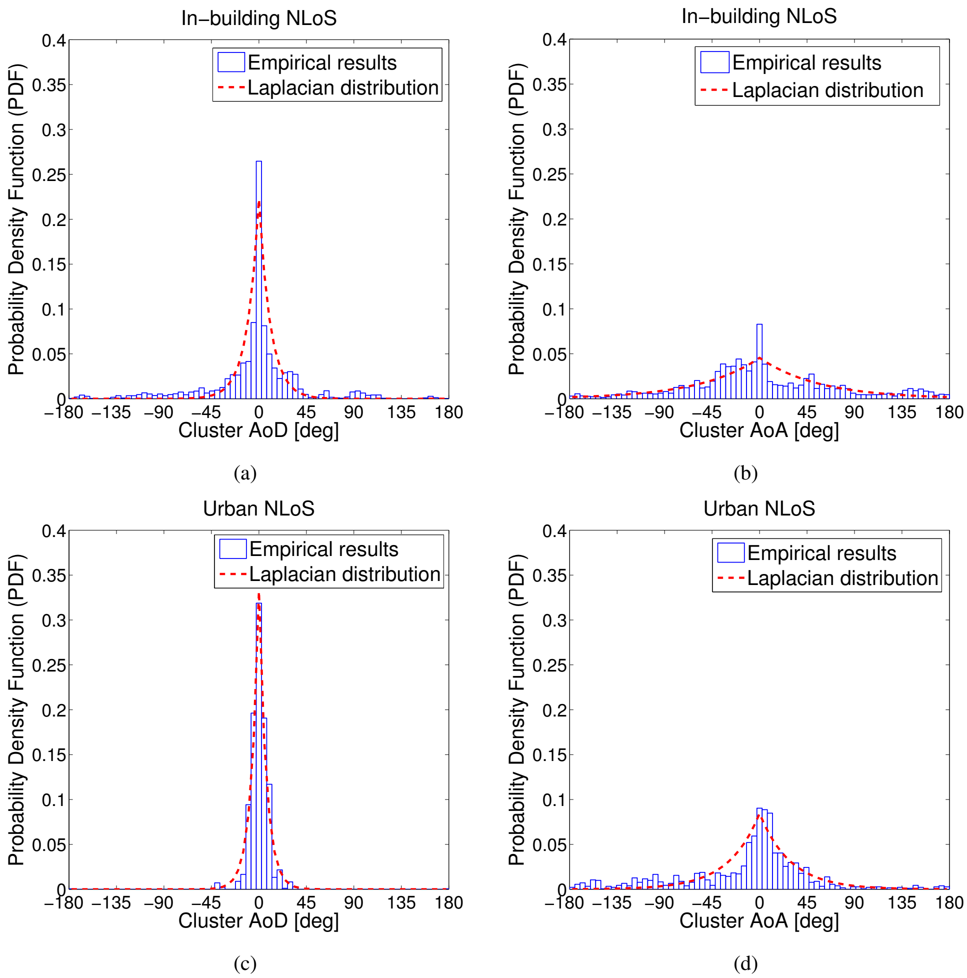

Fig. 9. Probability density functions of (a) cluster AoD and (b) AoA for the in-building NLoS channels, and (c) cluster AoD and (d) AoA for the urban NLoS channels.

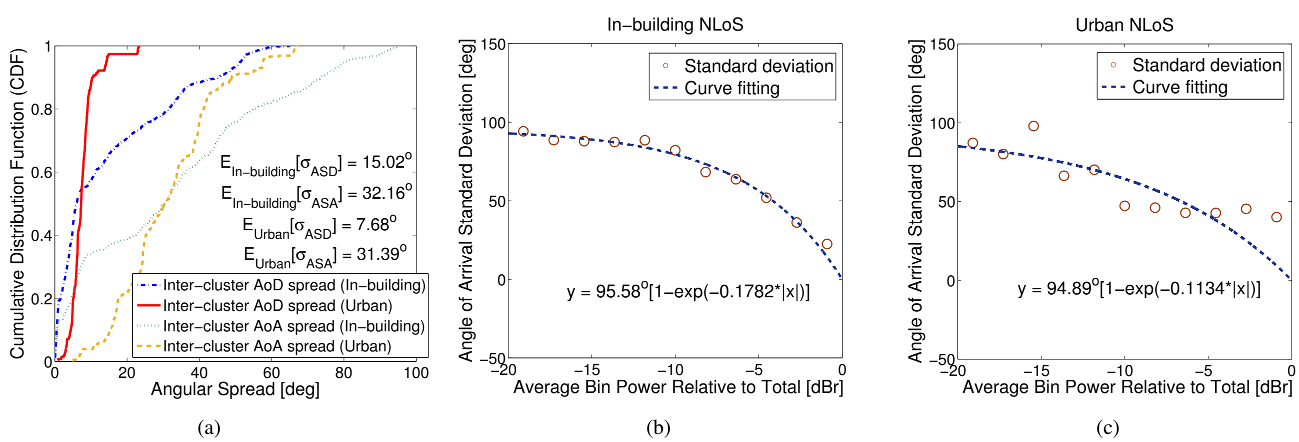

Fig. 10. (a) Cumulative distribution function of inter-cluster AoD/AoA spreads: both the in-building NLoS and urban NLoS environments. Angle of arrival standard deviations versus average bin power relative to total received power for (b) the in-building NLoS and (c) urban NLoS environments.

The AoA/AoD offsets can be modeled as random variables or as fixed values as long as the measured intra-cluster ASD and ASA are reproduced correctly. Figure 12 shows the PDFs of the measured intra-cluster AoDs and AoAs in the two environments. Similarly to the cluster AoD/AoA depicted in Fig. 9, a Laplacian distribution models the PDF best. The measured intra-cluster ASD and ASA of the in-building and urban environments have mean values $\{\sigma_{ASD,c} = E\left[\sigma_{ASD,k}\right], \sigma_{ASA,c} = E\left[\sigma_{ASA,k}\right]\}$, of $\{4.33^\circ, 5.94^\circ\}$ and $\{5.82^\circ, 15.56^\circ\}$, respectively. Note that intra-cluster ASs smaller than the beam width of the horn antennas on the Tx and Rx sides were roughly calculated and

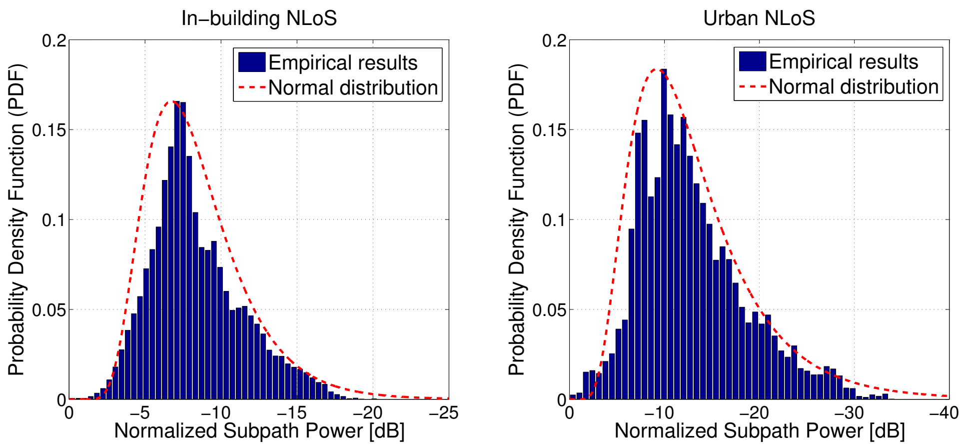

(a) (b)

Fig. 11. Probability density functions of normalized subpath powers for (a) the in-building NLoS and (b) urban NLoS environments.

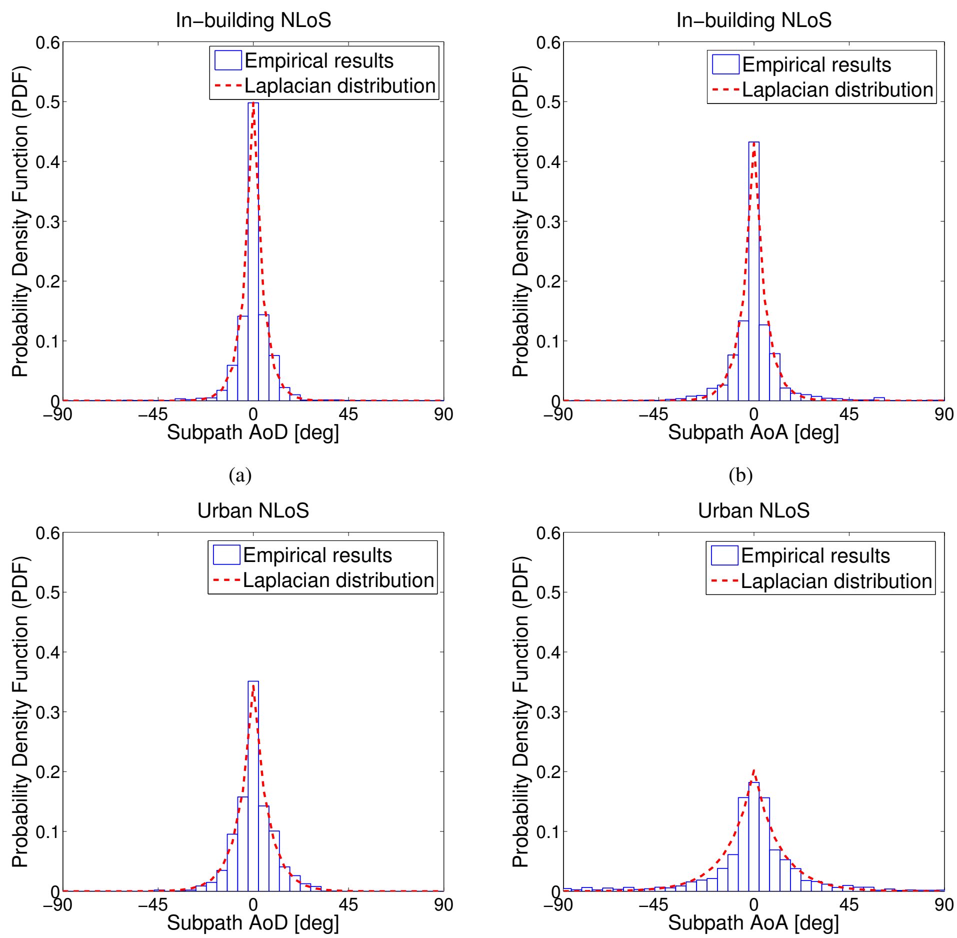

(a) (b) (c) (d)

Fig. 12. Probability density functions of intra-cluster angles for the NLOS in-building scenario: (a) AoD and (b) AoA, and for the NLOS urban scenario: (c) AoD and (d) AoA.

based on subpaths which appear across several adjacent angular bins; the subpaths were resolved in the delay domain owing to the large bandwidth of the sounder. If highly precise intra-cluster AS values are required for any specific application, it should be considered that the limited angular resolution of the channel sounder has an impact on the intra-cluster spreads. Thus, a ray-tracing analysis and/or measurements with a narrower beam width for our measurement scenarios would be needed to obtain more reliable intra-cluster spread values.

Similarly to the intra-cluster delays, the intra-cluster AoD/AoA can also be modeled as random variables or fixed values. The random intra-cluster AoD and AoA models are expressed by the PDFs of δ_{AoD} as following:

$$f_{\delta_{AoD}}\left(\delta_{AoD}\right) \triangleq \frac{1}{\sqrt{2}\sigma_{ASD,c}} \exp\left(-\frac{\sqrt{2}\left|\delta_{AoD}\right|}{\sigma_{ASD,c}}\right), \quad (9)$$

where $-\infty < \delta_{AoD} < \infty$; this also applies to the intra-cluster AoA model. The CDFs of $f_{\delta_{AoD}}\left(\delta_{AoD}\right)$ are denoted as $F_{\delta_{AoD}}\left(\delta_{AoD}\right)$. In the same manner used with the random intra-cluster delay model, it is necessary to define effective intervals for the intra-cluster AoD and AoA to limit the cluster size in the spatial domain, where constrained PDFs $f_{\delta'_{AoD}}\left(\delta'_{AoD}\right)$ are used to generate distinct clusters in the channel model outputs as follows:

$$f_{\delta'_{AoD}}\left(\delta'_{AoD}\right) \triangleq \begin{cases} \frac{f_{\delta_{AoD}}\left(\delta'_{AoD}\right)}{1-2\cdot F_{\delta_{AoD}}\left(-\delta_{AoD}^{\text{bound}}\right)}, & \left|\delta'_{AoD}\right| \leq \delta_{AoD}^{\text{bound}} \\ 0, & \left|\delta'_{AoD}\right| > \delta_{AoD}^{\text{bound}} \end{cases}, \quad (10)$$

where δ_{AoD}^{bound} is determined to satisfy

$$\sqrt{E\left[\delta'^{2}_{AoD}\right]} = c_2\sigma_{ASD,c}.$$

The constant c_2 is set to 0.95. The same model is applicable to the intra-cluster AoA.

E. Cross Correlation Properties between Channel Parameters

As observed in Section IV, log-normal distributions describe large scale parameters well. Moreover, large scale parameters, i.e., the inter-cluster ASD, ASA, DS (on the log scale) and shadow fading (SF, in dB) are generally correlated with each other [54]-[56]. These findings allow us to generate large scale parameters based on correlated Gaussian random variables. The cross correlation coefficient between random variables X and Y is obtained according to the following equation:

$$\rho\left(X,Y\right) = \frac{\sum_{n_s=1}^{N_s}\left(X_{n_s}-\bar{X}\right)\left(Y_{n_s}-\bar{Y}\right)}{\sqrt{\sum_{n_s=1}^{N_s}\left(X_{n_s}-\bar{X}\right)^2 \sum_{n_s^*=1}^{N_s}\left(Y_{n_s^*}-\bar{Y}\right)^2}}. \quad (11)$$

Here, X_{n_s} and Y_{n_s} denote the n_s-th measured samples for X and Y, and $\bar{X}$ and $\bar{Y}$ denote the sample means of X and Y with the set size of N_s, respectively. As an example, a set of scatter plots for large scale parameters in the in-building scenario is shown in Fig. 13, with the linear fitted line from the measured data. Table IV presents the cross correlation coefficients of the in-building and urban scenarios.

Based on our 28 GHz measurements, the cross correlations of large scale parameters tend to be similar in both the in-building and urban scenarios; negative cross correlations between SF and the other parameters are observed, while positive correlations are shown between ASD and DS, DS and ASA, and ASA and ASD. It can also be observed that the cross correlations between SF and other parameters are lower than those between DS and AS in all of the measured environments. Some discussions indicating the cross-correlation results in Table IV are as follows. First, a negative cross correlation is obtained between DS and SF; as observed in an earlier study [49], it is well known that when a signal whose power-delay spectrum has an exponential distribution (a decaying function) undergoes deep fading (negative SF), the power levels of the dominant paths are weakened, which leads to a uniform distribution (higher DS). Note that although the cross correlation value is slightly larger in the urban environment, where deep fading is relatively more likely to occur, the correlation values between SF and DS are not so large in the two scenarios. Second, between SF and ASA, a negative cross correlation is also observed. This situation is similar to the principle applied in the case of a correlation between SF and DS: as SF becomes smaller, ASA becomes larger. If a receiver is in an environment with more scattering and with more distant scatterers, such as a street crossing, a small negative or even positive cross correlation would be obtained (higher ASA). This finding coincides with the result showing that the negative correlation is more pronounced in the case of the urban measurement, where the scattering environment is more limited. This phenomenon can also be extended for ASD and SF.

Third, the observation that there is a positive cross correlation between DS and AS (ASD/ASA) is plausible because many signal components may broaden the delay and angular domains simultaneously. Due to the fact that a low AS (ASD/ASA) engenders a high correlation between received signals by spatially separated antennas and a low DS results in a wide coherence bandwidth, in terms of system design processes, space or frequency diversity gains may be highly correlated. Therefore, a positive correlation between DS and AS might mean that for achieving a particular diversity order, we can not add up the spatial and frequency diversity order, but have to anticipate that they can be simultaneously bad at the same time. However, it was found in this work that the cross correlations between DS and AS are much lower in urban measurements compared with in-building measurements. Finally, a positive cross correlation between ASA and ASD is observed, indicating that the mechanism causing angular (azimuthal) dispersion at the receiver is related to the mechanism leading to angular dispersion on the Tx side. In Table IV, the channel model parameters obtained in this work are also summarized.

V. Conclusion

In this work, radio channel measurements and analyses are conducted to explore the characteristics of mmWave channels, in particular in the 28 GHz band. A correlator-based channel sounder with automatically scanning horn antennas for 28 GHz was used to perform directional measurements. The omni-directional channels can be synthesized by aligning different directional PDPs using associated time stamps. A set of mmWave channel parameters based on a clustered channel model is presented for two important cellular scenarios, i.e., an urban microcell and an indoor open-hall mainly for NLoS scenarios. The sounding measurements were performed in the Korea Advanced Institute of Science and Technology (KAIST)

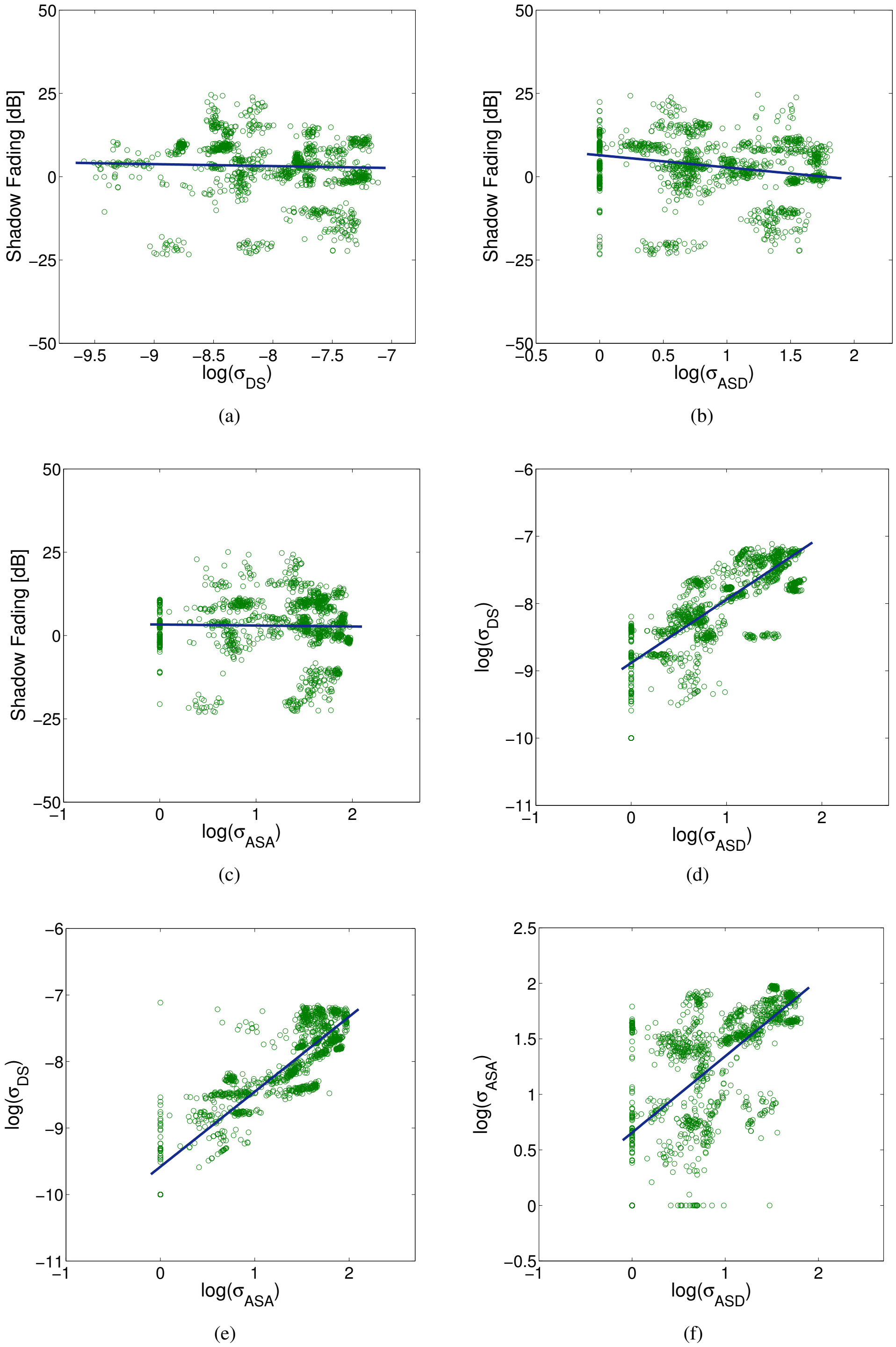

Fig. 13. Scatter plots of different large scale parameters for the in-building channels: (a) log(DS) and shadow fading in dB, (b) log(ASD) and shadow fading in dB, (c) log(ASA) and shadow fading in dB, (d) log(ASD) and log(DS), (e) log(ASA) and log(DS), and (f) log(ASD) and log(ASA).

campus and urban areas of Daejeon, South Korea. Extensive channel sounding campaigns in the NLoS in-building and urban environments led to statistically reliable channel parameters for the two environments at 28 GHz. We provide a detailed cluster analysis of multipath channels such as delay, angle and power distributions of the inter- and intra-cluster paths. The presented mmWave propagation characteristics including channel parameters will provide further understanding of mmWave radio channels and opportunities for designing mmWave communication systems.

Acknowledgment

This work was supported by Samsung Electronics Co., LTD.

References

[1] S. Hur, Y.-J. Cho, T. Kim, J. Park, A. F. Molisch, K. Haneda and M. Peter, “Wideband spatial channel model in an urban cellular environments at 28 GHz,” in *Proc. Eur. Conf. Antennas Propag. (EuCAP)*, Apr. 2015, pp. 1-5.

[2] W. Roh, J.-Y. Seol, J. Park, B. Lee, J. Lee, Y. Kim, J. Cho, K. Cheun, and F. Aryanfar, “Millimeter-wave beamforming as an enabling technology for 5G cellular communications: theoretical feasibility and prototype results,” *IEEE Commun. Mag.*, vol. 52, no. 2, pp. 106-113, Feb. 2014.

TABLE IV

CHANNEL MODEL PARAMETERS FOR THE IN-BUILDING AND URBAN SCENARIOS

Scenario		Indoor hotspot NLoS	UMi street canyon NLoS
Environment		KAIST campus	Daejeon
Delay spread [ns]	Inter-cluster	18.91	55.43
	Intra-cluster	3.90	12.86
AoD spread [degree]	Inter-cluster	15.02	7.68
	Intra-cluster	4.33	5.82
AoA spread [degree]	Inter-cluster	32.16	31.39
	Intra-cluster	5.94	15.56
Path loss	$\overline{n}_{CI}$	2.80	2.92
	α_{AB} [dB]	80.05	46.61
	β_{AB}	1.53	3.63
Shadow fading [dB]	ς_{CI}	6.18	9.89
	σ_{AB}	5.79	9.83
Cross correlation	$\rho\left(\log\sigma_{DS}, X_\sigma\right)$	-0.0995	-0.1293
	$\rho\left(\log\sigma_{ASD}, X_\sigma\right)$	-0.1569	-0.2244
	$\rho\left(\log\sigma_{ASA}, X_\sigma\right)$	-0.0195	-0.1293
	$\rho\left(\log\sigma_{ASD}, \log\sigma_{DS}\right)$	0.7926	0.5539
	$\rho\left(\log\sigma_{ASA}, \log\sigma_{DS}\right)$	0.8795	0.0685
	$\rho\left(\log\sigma_{ASD}, \log\sigma_{ASA}\right)$	0.6596	0.2303
Delay distribution		Exponential	
AoD distribution		Laplacian	
AoA distribution		Laplacian	
Number of clusters		4 (3.52)	5 (4.58)

[3] Z. Pi and F. Khan, "An introduction to millimeter-wave mobile broadband systems," *IEEE Commun. Mag.*, vol. 49, no. 6, pp. 101-107, Jun. 2011.

[4] S. Hur, T. Kim, D. Love, J. Krogmeier, T. Thomas, and A. Ghosh, "Millimeter wave beamforming for wireless backhaul and access in small cell networks," *IEEE Trans. Commun.*, vol. 61, no. 10, pp. 4391-4403, Oct. 2013.

[5] "http://www.nist.gov/ctl/upload/5G-millimeter-wave-channel-modelalliancev2. pdf."

[6] "https://www.metis2020.com/documents/deliverables/."

[7] "Study on channel model for frequency spectrum above 6 GHz (Relaease 14)," 3GPP TR 38.900 V14.0.0, Jun. 2016.

[8] "FCC Promotes Higher Frequency Spectrum for Future Wireless Technology," *MCI v. FCC. 515 F 2d 385*, Oct. 2015.

[9] A. F. Molisch, *Wireless Communications*, 2nd ed. IEEE Press - Wiley, 2011.

[10] Aalto University, BUPT, CMCC, Nokia, NTT DOCOMO, New York University, Ericsson, Qualcomm, Huawei, Samsung, Intel, University of Bristol, KT Corporation, University of Southern California, "5G channel model for bands up to 100 GHz," Oct. 2016, Tech. Rep. [Online]. Available: http://www.5gworkshops.com/5GCM.html

[11] A. Adhikary, E. A. Safadi, M. K. Samimi, R. Wang, G. Caire, T. S. Rappaport, and A. F. Molisch, "Joint spatial division and multiplexing for mm-Wave channels," *IEEE J. Select. Areas Commun.*, vol. 32, no. 6, pp. 1239-1255, Jun. 2014.

[12] Kyösti, et al., "WINNER II Channel Models," D1.1.2 V1.1, IST-4-027756 WINNER II Deliverable, Sep. 2007. [Online]. Available: http://www.ist-winner.org/WINNER2-Deliverables/D1.1.2v1.1.pdf

[13] "Study on 3D channel model for LTE (Relaease 12)," 3GPP TR 36.873 V12.0.0, Sep. 2014. [Online]. Available: http://www.3gpp.org/ftp/Specs/archive/36_series/36.873/36873-c00.zip

[14] M. Samimi, K. Wang, Y. Azar, G. N. Wong, R. Mayzus, H. Zhao, J. K. Schulz, S. Sun, F. Gutierrez Jr., and T. S. Rappaport, "28 GHz angle of arrival and angle of departure analysis for outdoor cellular communications using steerable-beam antennas in New York City," in *Proc. IEEE Veh. Technol. Conf. (VTC)*, Jun. 2013, pp. 1-6.

[15] T. S. Rappaport, S. Sun, R. Mayzus, H. Zhao, Y. Azar, K. Wang, G. N. Wong, J. K. Schulz, M. Samimi, and F. Gutierrez, "Millimeter wave mobile communications for 5G cellular: It will work!," *IEEE Access*, vol. 1, pp. 335-349, May 2013.

[16] T. S. Rappaport, G. R. MacCartney, M. K. Samimi, and S. Sun, "Wideband millimeter-wave propagation measurements and channel models for future wireless communication system design," *IEEE Trans. Commun.*, vol. 63, no. 9, pp. 3029-3056, Sep. 2015.

[17] M. K. Samimi and T. S. Rappaport, "Local multipath model parameters for generating 5G millimeter-wave 3GPP-like channel impulse response," in *Proc. Eur. Conf. Antennas Propag. (EuCAP)*, Apr. 2016, pp. 1-5.

[18] G. R. MacCartney Jr., M. K. Samimi, and T. S. Rappaport, "Omnidirectional path loss models in New York City at 28 GHz and 73 GHz," in *Proc. IEEE Int. Symp. Pers. Indoor Mobile Radio Commun. (PIMRC)*, Sep. 2014, pp. 227-231.

[19] M. K. Samimi and T. S. Rappaport, "3-D statistical channel models for millimeter-wave outdoor mobile broadband communication," in *Proc. IEEE Int. Conf. Commun. (ICC)*, Jun. 2015, pp. 2430-2436.

[20] R. J. Weiler, M. Peter, T. Khne, M. Wisotzki, and W. Keusgen, "Simultaneous millimeter-wave multi-band channel sounding in an urban access scenario," in *Proc. Eur. Conf. Antennas Propag. (EuCAP)*, May 2015, pp. 1-5.

[21] M. Sasaki, W. Yamada, T. Sugiyama, M. Mizoguchi, and T. Imai, "Path loss characteristics at 800 MHz to 37 GHz in urban street microcell environment," in *Proc. Eur. Conf. Antennas Propag. (EuCAP)*, May 2015, pp. 1-4.

[22] S. Hur, S. Baek, B. Kim, Y. Chang, A. F. Molisch, T. S. Rappaport, K. Haneda, and J. Park, "Proposal on millimeter-wave channel modeling for 5G cellular system," *IEEE J. Select. Topics Signal Processing*, vol. 10, no. 3, pp. 454-469, Apr. 2016.

[23] K. Haneda, N. Omaki, T. Imai, L. Raschkowski, M. Peter and A.

Roivainen, "Frequency-agile pathloss models in urban street canyons," *IEEE Trans. Antennas Propag.*, vol. 64, no. 5, pp. 1941-1951, May 2016.

[24] A. F. Molisch, A. Karttunen, S. Hur, J. Park, and J. Zhang, "Spatially consistent path loss modeling for millimeter-wave channels in urban environments," in *Proc. Eur. Conf. Antennas Propag. (EuCAP)*, Apr. 2016, pp. 1-5.

[25] A. Karttunen, A. F. Molisch, S. Hur, J. Park and J. Zhang, "Spatially consistent street-by-street path loss model for 28 GHz channels in urban environments," *IEEE Trans. Wireless Commun.*, Submitted.

[26] K. Haneda, J. Jarvelainen, A. Karttunen, M. Kyro and J. Putkonen, "A statistical spatio-temporal radio channel model for large indoor environments at 60 and 70 GHz," *IEEE Trans. Antennas Propag.*, vol. 63, no. 6, pp. 2694-2704, Jun. 2015.

[27] K. Haneda, "Channel models and beaforming at millimeter-wave frequency bands," *IEICE Trans. Commun.*, vol. E98-B, no. 5, pp. 755-772, May 2015.

[28] M. Steinbauer, A. F. Molisch, and E. Bonek, "The double-directional radio channel," *IEEE Antennas Propag. Mag.*, vol. 43, no. 4, pp. 51-63, Aug. 2001.

[29] S. Hur, Y.-J. Cho, J. Lee, N.-G. Kang, J. Park and H. Benn, "Synchronous channel sounder using horn antenna and indoor measurements on 28 GHz," in *Proc. IEEE Int. Black Sea Conf. on Commun. Netw. (BlackSeaCom)*, May 2014, pp. 83-87.

[30] J. Ko, S. Hur, S. Lee, Y. Kim, Y.-S. Noh, Y.-J. Cho, S. Kim, S. Bong, S. Kim, J. Park, D.-J. Park and D.-H. Cho, "28 GHz channel measurements and modeling in a ski resort town in pyeongchang for 5G cellular network systems," in *Proc. Eur. Conf. Antennas Propag. (EuCAP)*, Apr. 2016, pp. 1-5.

[31] J. Ko, K. Lee, Y.-J. Cho, S. Oh, S. Hur, N.-G. Kang, J. Park, D.-J. Park and D.-H. Cho, "Feasibility study and spatial-temporal characteristics analysis for 28 GHz outdoor wireless channel modelling," *IET Commun.*, vol. 10, no. 17, pp. 2352-2362, Nov. 2016.

[32] M. K. Samimi and T. S. Rappaport: "Synthesizing omnidirectional antenna patterns, received power and path loss from directional antennas for 5G millimeter-wave communications," in *Proc. IEEE Global Commun. Conf. (GLOBECOM) Workshop*, Dec. 2015, pp. 1-7

[33] M. Hata, "Empirical formula for propagation loss in land mobile radio services," *IEEE Trans. Veh. Thechnol.*, vol. 29, no. 3, pp. 317-325, Aug. 1980.

[34] R. Verdone, "Pervasive Mobile & Ambient Wireless Communications," in *COST 2100 Final Report*, Berlin: Springer, 2011.

[35] A. Karttunen, C. Gustafson, A. F. Molisch, R. Wang, S. Hur, J. Zhang, J. Park, "Path loss models with distance dependent weighted fitting and estimation of censored path loss data," *IET Microwaves Antennas Propag.*, Accepted.

[36] G. Maccartney, T. Rappaport, S. Sun, and S. Deng, "Indoor office wideband millimeter-wave propagation measurements and channel models at 28 and 73 GHz for ultra-dense 5G wireless networks," *IEEE Access*, vol. 3, pp. 2388-2424, Oct. 2015.

[37] H. Yang, M. H. A. J. Herben, and P. F. M. Smulders, "Impact of antenna pattern and reflective environment on 60 GHz indoor radio channel characteristics," *IEEE Antennas Wireless Propag. Lett.*, vol. 4, pp. 300-303, Sep. 2005.

[38] P. F. M. Smulders, "Statistical characterization of 60-GHz indoor radio channels," *IEEE Trans. Antennas Propag.*, vol. 57, no. 10, pp. 2820-2829, Oct. 2009.

[39] J. Jarvelainen, S. L. H. Nguyen, K. Haneda, R. Naderpour and U. T. Virk, "Evaluation of millimeter-wave line-of-sight probability with point cloud data," *IEEE Wireless Commum. Lett.*, vol. 5, no. 3, pp. 228-231, Jun. 2016.

[40] Report ITU-R M.2135, "Guidelines for evaluation of radio interface technologies for IMT-advanced," 2008.

[41] N. Costa and S. Haykin, *"Multiple-Input Multiple-Output Channel Models: Theory and Practice,"* New York: John Wiley & Sons, 2010.

[42] N. Czink, "The random-cluster model – a stochastic MIMO channel model for broadband wireless communication systems of the 3rd generation and beyond," In Institut für Nachrichtentechnik und Hochfrequenztechnik, Vienna, Technische Universität Wien, available at: http://publik.tuwien.ac.at/files/PubDat_112121.pdf

[43] D.-J. Kim, Y.-W. Park and D.-J. Park, "A novel validity index for determination of the optimal number of clusters," *IEICE Trans. Inf. Syst.*, vol. 38, no. 2, pp. 281-285, Feb. 2001.

[44] A. F. Molisch, H. Asplund, R. Heddergott, M. Steinbauer, and T. Zwick, "The COST 259 directional channel model - Part I: overview and methodology," *IEEE Trans. Wireless Commun.*, vol. 5, no. 12, pp. 3421-3433, Dec. 2006.

[45] H. Asplund, A. A. Glazunov, A. F. Molisch, K. I. Pedersen, and M. Steinbauer, "The COST 259 directional channel model - Part II: macrocells," *IEEE Trans. Wireless Commun.*, vol. 5, no. 12, pp. 3434-3450, Dec. 2006.

[46] A. L. Swindlehurst, E. Ayanoglu, P. Heydari, and F. Capolino, "Millimeter-wave massive MIMO: the next wireless revolution?," *IEEE Commun. Mag.*, vol. 52, no. 9, pp. 56-62, Sep. 2014.

[47] S. L. H. Nguyen, K. Haneda, J. Jarvelainen, A. Karttunen and J. Putkonen, "On the mutual orthogonality of millimeter-wave massive MIMO channels," *Proc. IEEE Veh. Technol. Conf. (VTC)*, May 2015, pp. 1-5.

[48] A. A. M. Saleh and R. A. Valenzuela, "A statistical model for indoor multipath propagation," *IEEE J. Select. Areas Commun.*, vol. 5, no. 2, pp. 128-137, Feb. 1987.

[49] L. J. Greenstein, V. Erceg, Y. S. Yeh, and M. V. Clark, "A new path-gain/delay-spread propagation model for digital cellular channels," in *IEEE Trans. Veh. Thechnol.*, vol. 46, no. 2, pp. 477-485, May 1997.

[50] G. R. MacCartney, Jr., M. K. Samimi, and T. S. Rappaport, "Exploiting directionality for millimeter-wave wireless system improvement," in *Proc. IEEE Int. Conf. Commun. (ICC)*, Jun. 2015, pp. 4019-4025.

[51] H. Iwai and Y. Karasawa, "Wideband propagation model for the analysis of the effect of the multipath fading on the near-far problem in CDMA mobile radio systems," *IEICE Trans. Commun.*, vol. 76-B, no. 2, pp. 342-354, Feb. 1993.

[52] "Spatial channel model for multiple input multiple output (MIMO) simulations," 3GPP TR 25.996 V11.0.0, Sep. 2012. [Online]. Available: http://www.3gpp.org/ftp/Specs/html-info/25996.htm

[53] G. Calcev, D. Chizhik, B. Göransson, S. Howard, H. Huang, A. Kogiantis, A. F. Molisch, A. L. Moustakas, D. Reed, and H. Xu, "A wideband spatial channel model for system-wide simulations," *IEEE Trans. Veh. Technol.*, vol. 56, no. 2, pp. 389-403, Mar. 2007.

[54] K. I. Pedersen, P. E. Mogensen, and B. H. Fleury, "A stochastic model of the temporal and azimuthal dispersion seen at the base station in outdoor propagation environments," *IEEE Trans. Veh. Thechnol.*, vol. 49, no. 2, pp. 437-447, Mar. 2000.

[55] K. I. Pedersen, P. E. Mogensen, B. H. Fleury, F. Frederiksen, and K. Olesen, "Analysis of time, azimuth and doppler dispersion in outdoor radio channels," in *Proc. ACTS Mobile Commun. Summit '97*, Aalborg, Denmark, pp. 308-313, Oct. 1997.

[56] A. Algans, K. I. Pedersen, and P. E. Mogensen, "Experimental analysis of the joint statistical properties of azimuth spread, delay spread, and shadow fading," in *IEEE J. Select. Areas Commun.*, vol. 20, no. 3, pp. 523-531, Apr. 2002.

Junghoon Ko received the B.S. degree from Kwangwoon University, Seoul, Korea, in 2010 and the M.S. degree in electrical engineering from the Korea Advanced Institute of Science and Technology (KAIST), Daejeon, Korea, in 2012. He is currently working toward the Ph.D. degree at the KAIST. His research interests include signal processing for wireless communications, statistical signal processing, 5G wireless communication networks, and millimeter-wave channel modeling.

Yeon-Jea Cho (M'16) received the B.S. degree from Kyungpook National University, Daegu, Korea, in 2010 and the M.S. and Ph.D. degrees in electrical engineering from the Korea Advanced Institute of Science and Technology, Daejeon, Korea, in 2011 and 2016, respectively. He is currently a Senior Research Engineer with Korea Telecom R&D center, Seoul. His research interests include statistical signal processing, 5G wireless communication networks, millimeter wave channel sounding, channel modeling, and cognitive radio networks.

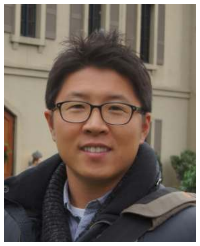

Sooyoung Hur (S'05 - M'13) received the B.S degree from Sogang University, Seoul, Korea, in 2005, and M.S. degree from Korea Advanced Institute of Science and Technology (KAIST), Daejeon, Korea in 2007, both in electrical engineering. He received a Ph.D in electrical and computer engineering from Purdue University, West Lafayette, IN in 2013. Since 2013 he has been with Samsung Electronics in the Communication Research Team. His current research interests are in physical layer communications and in particular channel measurements, cellular and mmWave communications, and signal processing for wireless communications, especially 5G communication technologies including standardization in 3GPP RAN and ITU-R IMT-Systems.

Taehwan Kim received the B.S. degree in radio science and engineering and M.S. degree in electrical engineering from Korea University, Seoul, South Korea, in 2007 and 2009, respectively. He is currently Senior Research Engineer with LG Electronics. His research interests include fifth-generation wireless communication networks, millimeter-wave communications, and beamforming.

Jeongho Park received his Ph.D. degree in Electronic Engineering at Yonsei University. Since he joined Samsung Electronics in 2005, he has mainly been engaged in research and development of wireless communications. Standardization is also his interest including IEEE 802, 3GPP RAN and ITU-R IMT-Systems. Currently, Dr. Jeongho Park is the director of Communications Research Team at Samsung Electronics Mobile Communications Business and his research interest includes 5G technologies and cellular internet of things (IoT).

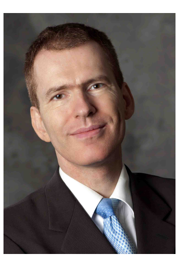

Andreas F. Molisch (S'89 - M'95 - SM'00 - F'05) received the Dipl. Ing., Ph.D., and habilitation degrees from the Technical University of Vienna, Vienna, Austria, in 1990, 1994, and 1999, respectively. He subsequently was with AT&T (Bell) Laboratories Research (USA); Lund University, Lund, Sweden, and Mitsubishi Electric Research Labs (USA). He is now a Professor and the Solomon-Golomb - Andrew-and-Erna Viterbi Chair at the University of Southern California, Los Angeles. His current research interests are the measurement and modeling of mobile radio channels, multi-antenna systems, wireless video distribution, ultra-wideband communications and localization, and novel modulation formats. He has authored, coauthored, or edited four books (among them the textbook Wireless Communications, Wiley-IEEE Press), 19 book chapters, more than 200 journal papers, some 300 conference papers, as well as more than 80 patents and 70 standards contributions.

Dr. Molisch has been an Editor of a number of journals and special issues, General Chair, Technical Program Committee Chair, or Symposium Chair of multiple international conferences, as well as Chairman of various international standardization groups. He is a Fellow of the National Academy of Inventors, Fellow of the AAAS, Fellow of the IET, an IEEE Distinguished Lecturer, and a member of the Austrian Academy of Sciences. He has received numerous awards, among them the Donald Fink Prize of the IEEE, and the Eric Sumner Award of the IEEE.

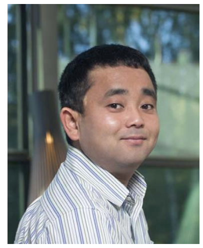

Katsuyuki Haneda (S'03 - M'07) received the Doctor of Engineering from the Tokyo Institute of Technology, Tokyo, Japan, in 2007. Dr. Haneda is presently an associate professor in Aalto University School of Electrical Engineering. He is the recipient of the best paper award of the antennas and propagation track in the IEEE 77th Vehicular Technology Conference (VTC2013-Spring), Dresden, Germany, and of the best propagation paper award in the 7th European Conference on Antennas and Propagation (EuCAP2013), Gothenburg, Sweden. Dr. Haneda has been an associate editor of the IEEE Transactions on Antennas and Propagation between 2012 and 2016, and of an editor of the IEEE Transactions on Wireless Communications since 2013. He has also been an active member of a number of European COST Actions, e.g., CA15104 "Inclusive Radio Communication Networks for 5G and beyond (IRACON)", where he is a co-chair of a disciplinary working group on radio channels. His current research activity includes high-frequency radios such as millimeter-wave and beyond, wireless for medical, post-disaster scenarios and internet-of-things, and in-band full-duplex radio technologies.

Michael Peter received the Diploma degree in Electrical Engineering and Information Technology from the University of Karlsruhe, Germany, in 2004. In 2005 he joined the Fraunhofer Heinrich Hertz Institute in Berlin, where he has been deeply involved in various national and European projects on 60 GHz and millimeter-wave communications, e.g. EASY-A, WiONet, MiWEBA and mmMAGIC. His research activities focus on millimeter-wave channel measurements and modeling, and physical layer design of wireless broadband communication systems. Michael Peter is author and co-author of more than 60 scientific papers.

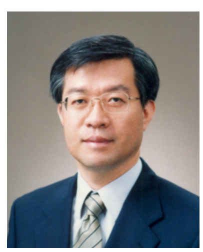

Dong-Jo Park (M'86) received the B.S. degree from Seoul National University, Seoul, Korea, in 1976 and the M.S. and Ph.D. degrees in electrical engineering from the University of California, Los Angeles, in 1981 and 1984, respectively. From 1984 to 1985, he was a Senior Researcher with the Electronics and Telecommunications Research Institute, Daejeon, Korea. He is currently a Professor with the School of Electrical Engineering, Korea Advanced Institute of Science and Technology, Daejeon. His research interests include multimedia signal processing, 5G wireless communications, channel and target identification in mmWave and long-wave Infrared bands, convex optimization and machine learning.

Dong-Ho Cho (M'85 - SM'00) received a Ph.D. degree in Electrical Engineering from KAIST in 1985. From 1987 to 1997, he was a Professor in the Dept. of Computer Engineering at Kyunghee University. Since 1998, he has been a professor in the School of Electrical Engineering of KAIST, and he was a Director of KAIST Institute for Information Technology Convergence from 2007 to 2011. He has been a director of KAIST Online Electric Vehicle Project since 2009 and he was a head of The Cho Chun Shik Graduate School for Green Transportation from 2010 to 2015. He was also an ICC(IT Convergence Campus) vice president of KAIST from 2011 to 2013. His research interests include mobile communication, online electric vehicle system based on wireless power transfer, and bioinformatics.